

On the inference of stellar ages and convective-core properties in main-sequence solar-like pulsators

I. M. Brandão^{1*}, M. S. Cunha¹ and J. Christensen-Dalsgaard²

¹*Centro de Astrofísica and Faculdade de Ciências, Universidade do Porto, Portugal, Rua das Estrelas, 4150-762 Porto, Portugal*

²*Stellar Astrophysics Centre, Department of Physics and Astronomy, Aarhus University, Ny Munkegade 120, DK-8000 Aarhus C, Denmark*

Accepted 2013 November 29. Received 2013 November 5; in original form 2013 July 18

ABSTRACT

Particular diagnostic tools may isolate the signature left on the oscillation frequencies by the presence of a small convective core. Their frequency derivative is expected to provide information about convective core's properties and stellar age. The main goal of this work is to study the potential of the diagnostic tools with regard to the inference of stellar age and stellar core's properties. For that, we computed diagnostic tools and their frequency derivatives from the oscillation frequencies of main-sequence models with masses between 1.0 and 1.6 M_{\odot} and with different physics. We considered the dependence of the diagnostic tools on stellar age and on the size of the relative discontinuity in the squared sound speed at the edge of the convectively unstable region. We find that the absolute value of the frequency derivatives of the diagnostic tools increases as the star evolves on the main sequence. The fraction of stellar main-sequence evolution for models with masses $> 1.2 M_{\odot}$ may be estimated from the frequency derivatives of two of the diagnostic tools. For lower mass models, constraints on the convective core's overshoot can potentially be derived based on the analysis of the same derivatives. For at least 35 per cent of our sample of stellar models, the frequency derivative of the diagnostic tools takes its maximum absolute value on the frequency range where observed oscillations may be expected.

Key words: asteroseismology – stars: fundamental parameters – stars: oscillations – stars: solar-type.

1 INTRODUCTION

According to stellar structure theory, stars slightly more massive than the Sun ($M > 1.0 M_{\odot}$) may develop a convective core at some stage of their evolution on the main sequence. This occurs when radiation can no longer transport the amount of energy produced by nuclear burning in the internal regions of a star. For these stars hydrogen burning happens primarily through the CNO cycle, which has a strong dependence on the temperature. Convection is then the most effective process to transport the energy, hence a convective core is present. Since convection implies chemical mixing, the evolution of these stars is severely influenced by the presence and the extent of the convective core.

Models of an intermediate-mass star ($1 M_{\odot} < M \leq 2 M_{\odot}$) with a convective core show that the extent in mass of the convective core does not remain constant during the evolution of the star. It increases during the initial stages of evolution before beginning to decrease, later on. Also, some physical ingredients such as the convective-core overshoot, if present, will influence the extent and evolution of the convective core.

A convective core is believed to be homogeneously mixed

since the time-scale for mixing of elements is much shorter than the nuclear time-scale. Thus, if diffusion is not taken into account, the growing core causes a discontinuity in the composition at the edge of the core (Mitalas 1972; Saio 1975), with a consequent density discontinuity. If diffusion is present, instead of a discontinuity, there will be a very steep gradient in the chemical abundance and density at the edge of the convective core. Moreover, a retreating core leaves behind a non-uniform chemical profile (Faulkner & Cannon 1973) causing also a very steep gradient in the chemical abundance.

This paper concerns the study of the properties of the convective cores in main-sequence models of solar-like pulsators. One of the main goals of inferring information of the deepest layers of stars is to improve the description of particular physical processes such as diffusion and convective overshoot, in stellar evolution codes. That, in turn, will improve the mass and age determinations derived from asteroseismic studies. This work presented here is driven, in particular, by the following questions: can we detect the signature of a small convective core on the oscillation frequencies of solar-like pulsators for which photometric data with the quality such as that of the NASA *Kepler* satellite (Borucki et al. 2010) exist? What is the dependence of this signature on the stellar mass and physical parameters? What is the precision required on the individual frequencies in order to detect the signature of a convective core?

* E-mail: isa@astro.up.pt

Will the detection of such a signature provide information about the stellar age?

To address these questions, we will focus on the analysis of a number of seismic diagnostic tools presented in Section 2. These diagnostic tools were computed for a set of main-sequence solar-like models through a method described in Section 3. In Section 4, we present our results and in Section 5, we conclude.

2 DIAGNOSTIC TOOLS

The oscillation frequencies of a pulsating star depend not only on its global properties, such as the mass and radius, but also on the details of its internal structure, including any sharp structural variations, such as those that are present at the borders of convectively unstable regions. Different combinations of low-degree p modes have been shown to probe the interior of stars (e.g. Christensen-Dalsgaard 1984). Among these, the most commonly used are the large frequency separation defined as the difference in frequency of modes of the same degree, l , and consecutive radial order, n , $\Delta\nu_{n,l} = \nu_{n+1,l} - \nu_{n,l}$ (e.g., Christensen-Dalsgaard, Gough & Morgan 1979a,b), and the small frequency separation between modes of degrees $l = 0$ and 2, $d_{02} = \nu_{n,0} - \nu_{n-1,2}$ (e.g. Gough 1983). In addition, Roxburgh & Vorontsov (2003) proposed smooth five-points small frequency separations, d_{01} and d_{10} , as a diagnostic of stellar interiors. These small separations are defined by

$$d_{01}(n) = \frac{1}{8}(\nu_{n-1,0} - 4\nu_{n-1,1} + 6\nu_{n,0} - 4\nu_{n,1} + \nu_{n+1,0}) \quad (1)$$

$$d_{10}(n) = -\frac{1}{8}(\nu_{n-1,1} - 4\nu_{n,0} + 6\nu_{n,1} - 4\nu_{n+1,0} + \nu_{n+1,1}). \quad (2)$$

All these diagnostic tools are, however, affected by the poorly modelled outer layers of stars. Nevertheless, Roxburgh & Vorontsov (2003) demonstrated that the effect of the outer stellar regions in the oscillation frequencies is cancelled out when one considers the ratios of these diagnostics (see also Roxburgh & Vorontsov 2004; Oti Floranes, Christensen-Dalsgaard & Thompson 2005; Roxburgh 2005). These ratios are defined by

$$r_{01}(n) = \frac{d_{01}(n)}{\Delta\nu_{n,1}}, \quad r_{10} = \frac{d_{10}(n)}{\Delta\nu_{n+1,0}}, \quad (3)$$

$$r_{02}(n) = \frac{d_{02}(n)}{\Delta\nu_{n,1}}, \quad (4)$$

and d_{02} is the small frequency separation previously defined. While d_{02} , d_{01} , d_{10} and the corresponding ratios probe the inner regions of the star, they do not isolate the signature left of the oscillation frequencies by the region of rapid structural variation associated with the edge of a convective core. An illustration of that structural variation is shown in Fig. 1, in terms of its impact in the sound-speed profile. The functional form of the corresponding signature on the frequencies was derived by Cunha & Metcalfe (2007) based on the properties of the oscillations of stellar models slightly more massive than the Sun. The authors assumed that this signature is caused by the discontinuity in the composition and hence in the sound speed at the edge of the growing convective core. They showed that the following combination of oscillation frequencies is sensitive to the properties of the sound-speed discontinuity, and is also capable of isolating the consequent perturbation to the oscillation frequencies:

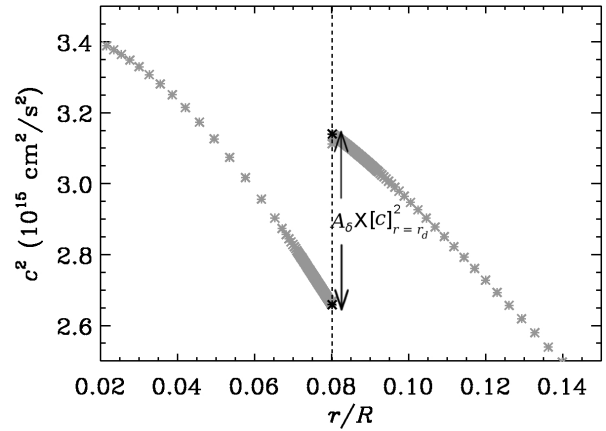


Figure 1. The square of the sound speed in the innermost regions of a $1.4 M_{\odot}$ model with an age of 1.56 Gyr computed with solar metallicity and assuming an overshoot from the convective core of $\alpha_{\text{OV}} = 0.1$. The dashed vertical line corresponds to the location of the discontinuity where the sound-speed derivative is maximum. The two black star symbols mark the position of the two extremes of the discontinuity, that are used to compute its amplitude in an automated manner.

$$dr_{0213} = 6 \left(\frac{D_{02}}{\Delta\nu_{n-1,1}} - \frac{D_{13}}{\Delta\nu_{n,0}} \right). \quad (5)$$

This diagnostic tool corresponds to a difference of ratios between the scaled small separations, $D_{l,l+2} \equiv (\nu_{n,l} - \nu_{n-1,l+2})/(4l + 6)$, and the large separations, $\Delta\nu_{n,l}$, for different combinations of mode degrees. Note that the authors originally defined this diagnostic tool without the factor 6. However, since the relation between the perturbation and the scaled small separations has a factor 6, we opted to include it here in the definition of dr_{0213} . More recently, Cunha & Brandão (2011) improved the analysis presented in Cunha & Metcalfe (2007), by considering a different expression to describe the sound-speed variation at the edge of the growing convective core, which is more in line with the variation observed from the equilibrium models. Moreover, they showed that the frequency derivative of the diagnostic tool dr_{0213} can potentially be used to infer the amplitude of the relative sound-speed variation at the edge of the growing convective core, $A_{\delta} \equiv [\delta c^2/c^2]_{r=r_d}$, with r_d being the radial position at which the discontinuity in the sound speed occurs (cf. Fig. 1), and c^2 at $r = r_d$ is the highest of the two c^2 values at the discontinuity. The disadvantage of this diagnostic tool is that it requires the observation of modes of degree up to 3.

In this work, we study the behaviour of the diagnostic tools defined by Eqs. (3)-(5). For that, we derived these tools for a set of stellar models considering a large parameter space. We then compare the frequency behaviour of the three diagnostic tools and consider their potential concerning the inference about the properties of stellar cores and the inference of stellar ages.

3 METHOD

3.1 Grids of models

We started by computing a set of evolutionary tracks with the ‘Aarhus STellar Evolution Code’ (ASTEC; Christensen-Dalsgaard 2008a). The models were calculated using the most up-to-date

Table 1. Parameters used to compute the evolutionary tracks. M/M_{\odot} is the mass in solar units, Z/X is the initial ratio of heavy elements to hydrogen abundances and Y the helium abundance. α_{ML} is the mixing-length parameter and α_{OV} the core overshoot parameter. We considered $(Z/X)_{\odot} = 0.0245$ for the Sun (Grevesse & Noels 1993).

| Parameter | Grid I | Grid II |
|----------------------|---------------------|---------------------|
| M/M_{\odot} | 1.0-1.6 (0.1 steps) | 1.0-1.6 (0.1 steps) |
| Z/X | 0.0245 | 0.0079, 0.0787 |
| Y | 0.278 | 0.255, 0.340 |
| α_{ML} | 1.8 | 1.8 |
| α_{OV} | 0.0-0.2 (0.1 steps) | 0.1 |

OPAL 2005 equation-of-state tables¹ (Rogers & Nayfonov 2002), OPAL95 opacities (Iglesias & Rogers 1996) complemented by low-temperature opacities from Ferguson et al. (2005). The opacities were calculated with the solar mixture of Grevesse & Noels (1993), and the Nuclear Astrophysics Compilation of REaction Rates (NACRE; Angulo et al. 1999). Convection was treated according to the standard mixing-length theory from Böhm-Vitense (1958), where the characteristic length of turbulence, called the mixing length l_{ML} , scales directly with the local pressure scale-height, H_p , as $l_{\text{ML}} = \alpha_{\text{ML}} H_p$, with $\alpha_{\text{ML}} > 1$. Overshooting (OV) exists when the convective movements of the gas in the convectively unstable regions cause extra mixing beyond the border of such regions. In our work, we only considered convective-core overshoot. In practice, since the core can be very small, ASTEC assumes $\alpha_{\text{OV}} \min(r_{\text{core}}, H_p)$, where r_{core} is the radius of the convective core. Regarding the atmosphere, we considered an atmospheric temperature versus optical depth relation which is a fit to the quiet-sun relation of Vernazza, Avrett & Loeser (1976). Diffusion and settling were not taken into account.

All of the evolutionary tracks computed contain a fixed number of models, not equally spaced in time, from the zero-age main sequence (ZAMS) to the post-main sequence. The parameter space that we considered in the modelling is shown in Table 1.

We constructed two grids of evolutionary tracks, Grid I and Grid II. For the former, we considered solar metallicity, i.e. $[\text{Fe}/\text{H}] = 0$, where $(Z/X)_{\odot} = 0.0245$ for the Sun (Grevesse & Noels 1993), and varied α_{OV} , while in Grid II, we fixed $\alpha_{\text{OV}} = 0.1$ and considered two extreme values for the metallicity, namely $[\text{Fe}/\text{H}] = -0.5$ and $[\text{Fe}/\text{H}] = 0.5$. To convert from $[\text{Fe}/\text{H}]$ to the initial ratio of heavy elements to hydrogen abundances, Z/X , we used the relation $[\text{Fe}/\text{H}] = \log(Z/X) - \log(Z/X)_{\odot}$, where $[\text{Fe}/\text{H}]$ is the star's metallicity, Z and X are all elements heavier than helium and hydrogen mass fractions, respectively, and $(Z/X)_{\odot}$ is the ratio for the solar mixture. The value of helium, Y , was obtained from the relation $Y = Y_p + Z dY/dZ$, where Y_p is the abundance of helium produced during primordial nucleosynthesis and dY/dZ is the helium to metal enrichment ratio. Considering $dY/dZ = 2$ (see, e.g., Casagrande 2007) and using the solar values of $(Z/X)_{\odot} = 0.0245$ (Grevesse & Noels 1993) and $Y_{\odot} = 0.278$ (Serenelli & Basu 2010) we found $Y_p = 0.2435$. Using $dY/dZ = 2$ and $Y_p = 0.2435$, and fixing Z , we derive Y .

We focused our work on intermediate-mass models, i.e. $1.0 M_{\odot} \leq M \leq 1.6 M_{\odot}$, because it is in this mass range that we expect main-sequence stars to show solar-like pulsations. We fixed the mixing-length parameter to 1.8. We note that changing the

mixing length parameter does not affect the convective core. In this region, the temperature gradient takes approximately its adiabatic value and is, therefore, independent of the details of the theory of convection. The values for the metallicity were chosen so that they comprise those derived for the solar-like stars observed by the *Kepler* satellite. The value of the convective overshoot for stars with masses $M < 1.7 M_{\odot}$ is quite unknown with literature values of α_{OV} ranging from 0.00 to 0.25 (Ribas, Jordi & Giménez 2000). We note that recent modelling of the *Kepler* main-sequence solar-like pulsator KIC 1200950 (also known as Dushera within the Kepler Asteroseismic Science Consortium), with an inferred mass of around $1.5 M_{\odot}$, required the presence of mixing beyond the boundary of its formal convective core (Silva Aguirre et al. 2013). We considered values for the convective-core overshoot between 0.0 and 0.2. Since our goal was only to study the dependence of the diagnostic tools on the input parameters, we did not construct refined grids.

3.2 Models selection

Each evolutionary track contains up to 200 models within the main-sequence phase, defined here as models with hydrogen abundance in the core $X_c > 10^{-2}$. The true number of models depends mainly on the mass associated with the track. Rather than analysing all the ≤ 200 models, we considered 12 models along the main-sequence phase that are equally spaced in $\log g$, $\log T_{\text{eff}}$ and $\log(L/L_{\odot})$. To select the 12 models, we started by computing the total parameter distance, $d_{\text{tot,param}}$, that a given model travels along the main sequence in a 3D space with the following parameters: $\log g$, $\log T_{\text{eff}}$ and $\log(L/L_{\odot})$. This distance is defined by

$$d_{\text{tot,param}} = \sum_{i=1}^{N-1} d_{i,\text{param}}, \quad (6)$$

and,

$$d_{i,\text{param}} = \left([\log g(i+1) - \log g(i)]^2 + [\log T_{\text{eff}}(i+1) - \log T_{\text{eff}}(i)]^2 + [\log(L/L_{\odot})(i+1) - \log(L/L_{\odot})(i)]^2 \right)^{1/2}, \quad (7)$$

where N is the total number of main-sequence models in each evolutionary track. The total distance was equally divided in 12 segments, and the 12 models were chosen such as to have their $\log g$, $\log T_{\text{eff}}$, and $\log(L/L_{\odot})$ the closest to the respective values for the 12 segments. Fig. 2 shows the Hertzsprung-Russell (HR) diagram for a set of main-sequence models with mass varying between 1.0 and 1.6 M_{\odot} , with solar metallicity and no convective-core overshoot. The 12 models are represented by the black star symbol. In this plot, the models shown are not equally spaced since, for clarity, the third dimension, namely $\log g$, is not represented.

For the 12 models within each track we computed oscillation frequencies using the Aarhus adiabatic oscillation code (ADIPLS; Christensen-Dalsgaard 2008b).

3.3 Diagnostic tools from models

In the case of stars with convective cores, we expect that the frequency derivatives of the diagnostic tools taken at their maximum absolute value are a measure of the amplitude of the discontinuity in the sound speed at the edge of the growing convective core (Cunha & Brandão 2011) and, hence, that they are strongly sensitive to the stellar age. An example of how the frequency derivative of dr_{0213} at its maximum absolute value changes during the

¹ OPAL tables available at http://opalopacity.llnl.gov/EOS_2005/.

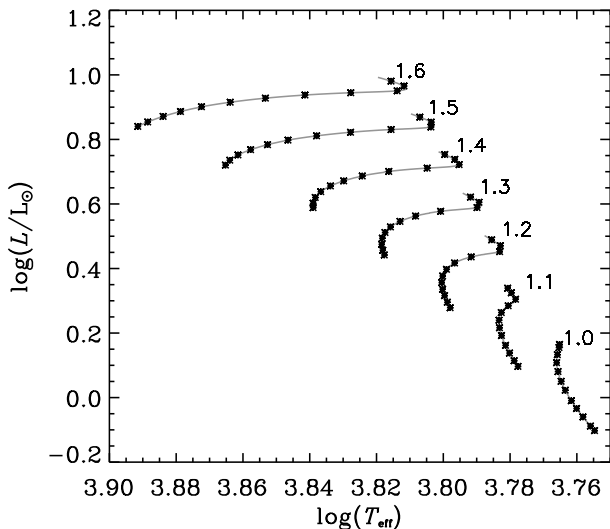


Figure 2. The HR diagram for a set of models with solar metallicity, $Z/X = 0.0245$, and no convective-core overshoot. The models were evolved from the ZAMS to the post-main sequence. Each evolutionary track contains 300 models at different evolutionary stages. Since the number of the computed models is fixed and the time step varies with mass and also along the evolution, the exact position of the last model of each evolutionary track depends on its mass. The numbers at the end of each evolutionary track correspond to the mass, in solar units. The 12 selected models within each evolutionary track are shown by a star symbol (see the text for details).

main-sequence evolution is shown in Fig. 3. It is quite clear that the absolute value of the derivative increases with age. Nevertheless, it is also clear from inspection of the figure that the frequency at which the absolute value of the derivative reaches its maximum is not always below the acoustic cut-off frequency, ν_c , i.e., below the maximum frequency such that acoustic waves are expected to be contained within the star). Consequently, some limitations are to be expected when trying to use the frequency derivatives of the seismic diagnostics tools as a way for determining stellar ages.

With the above in mind, we shall consider two different tasks in our study. First, we shall verify how strongly related are the frequency derivatives of the diagnostic tools taken at their maximum absolute value and the amplitude of the discontinuity in the sound speed at the edge of the convective core, using all models in our grid. For that, we will require that the oscillation frequencies in each model cover the region where the maximum absolute value of the derivatives is placed. Consequently, we apply a full reflective outer boundary condition in ADIPLS, expressed by $\delta p = 0$, where δp is the Lagrangian perturbation to the pressure, to obtain eigenfrequencies above the acoustic cut-off frequency. Later, we consider the observational impact of our results, by analysing the subset of models for which the maximum absolute value of the derivatives is below the acoustic cut-off frequency.

For practical purposes we introduce here a new quantity $S\{i\}$, which we shall name ‘slope’, which is a measure of the frequency derivative of a diagnostic tool ‘ i ’, at its maximum absolute value. To calculate the slopes of the diagnostic tools we proceed as follows: we start by inspecting the behaviour of the diagnostic tool dr_{0213} as a function of frequency to determine the frequency ν_{slope} at which the maximum absolute value of the derivative of dr_{0213} is placed and identify the corresponding radial order, n_{slope} . We then

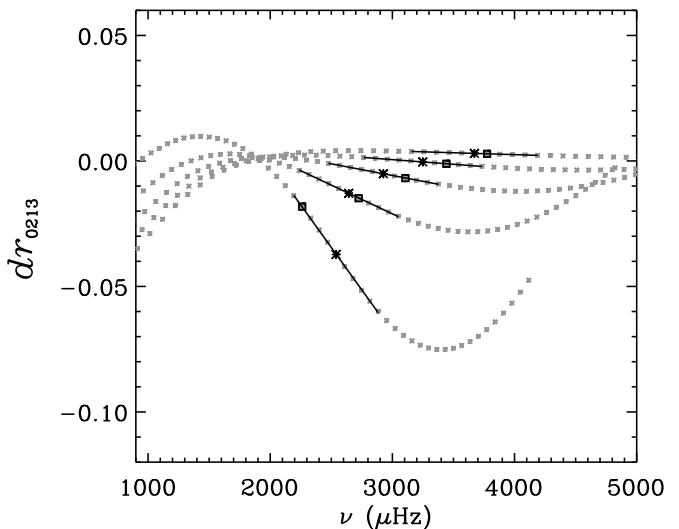


Figure 3. The diagnostic tool dr_{0213} as a function of frequency, ν , for a sequence of $1.3 M_{\odot}$ models with solar metallicity and without core overshoot. The different curves correspond to models with different ages, the most evolved model being the one with the largest absolute value of the derivative. The dark stars represent the frequencies at which the derivative takes its largest absolute value, for each model, and the straight black lines that cross that minima correspond to the region of approximately constant derivative (where the slopes are computed). The squares represent the acoustic cut-off frequency, ν_c , computed for each model. Note that for the oldest model, the region of constant derivative is above the cut-off frequency for the physics considered in our models.

perform a linear least-squares fit to the 10 frequencies of modes of consecutive radial orders, n , centred on n_{slope} . The slope of the diagnostic tool dr_{0213} around ν_{slope} is given by the linear coefficient obtained from this linear fit. The slopes of the diagnostic tools d_{01} , d_{10} and d_{02} , and their respective ratios, are computed in the same range of frequency as considered for dr_{0213} . Note that in relation to the quantities d_{01} and d_{10} , they are both five-point combination of modes of degrees $l = 0$ and 1, the first centred on modes of degree $l = 0$ and the second on modes of degree $l = 1$. In practice, we consider these two quantities together, denoting the concatenation of the two, appropriately ordered in frequency, by d_{010} , and the corresponding ratios by r_{010} . For this quantity, the slope is also determined in the same frequency range as that considered for dr_{0213} , but instead of 10, 20 frequencies are used. In Fig. 4, we show as an example, the diagnostic tools dr_{0213} , r_{010} and r_{02} computed for a $1.4 M_{\odot}$ model without overshoot and with solar metallicity at an age of 1.29 Gyr, and the frequency region considered in the computation of the slopes.

To have an estimation of the error associated with the slope computed for each diagnostic tool, we chose seven models with different values for the mass and input physics, and with different values of A_{δ} . For these models, we randomly generated 10 000 sets of model frequencies within the error, assuming a relative error of 10^{-4} for each individual frequency. For each generation, we computed the slopes in the same manner as described above. We then computed the mean of the 10 000 values obtained for the slopes and the standard deviation was considered to be our error estimation for the slopes of the diagnostic tools.

As mentioned above, models that have a convective core show

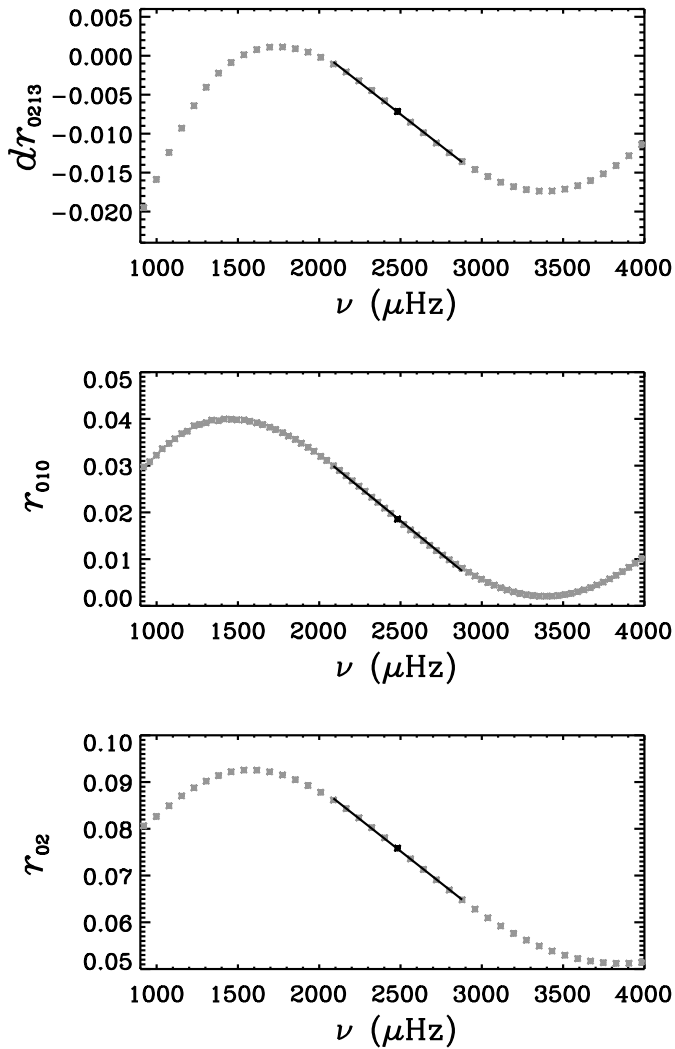


Figure 4. The three diagnostic tools, namely dr_{0213} (upper panel), r_{010} (middle panel) and r_{02} (lower panel) as a function of frequency, computed for a $1.4 M_{\odot}$ model without core overshoot and with solar metallicity. This model has an age of 1.29 Gyr and corresponds to the sixth model of the $1.4 M_{\odot}$ evolutionary track of Fig. 2.

a structural discontinuity at the edge of the convectively unstable region. Here, we aim at studying the relation between the relative amplitude A_{δ} of the discontinuity in the squared sound speed and the slopes of the diagnostic tools, $S\{i\}$. Thus, for the models for which we computed the diagnostic tools and that have a convective core, we also computed A_{δ} . To compute the latter, we started by identifying the location (in terms of r/R) of the discontinuity in c^2 . To do so, we identified the maximum value of the derivative of the squared sound speed in the inner regions of the models. This maximum value was used to determine the precise location of the discontinuity in an automated manner, for all models. With that we were able to automatically compute the actual amplitude of the sound-speed discontinuity by measuring the difference between the maximum and minimum values of c^2 at the discontinuity. These two values are shown, as an example, by the two black stars in Fig. 1.

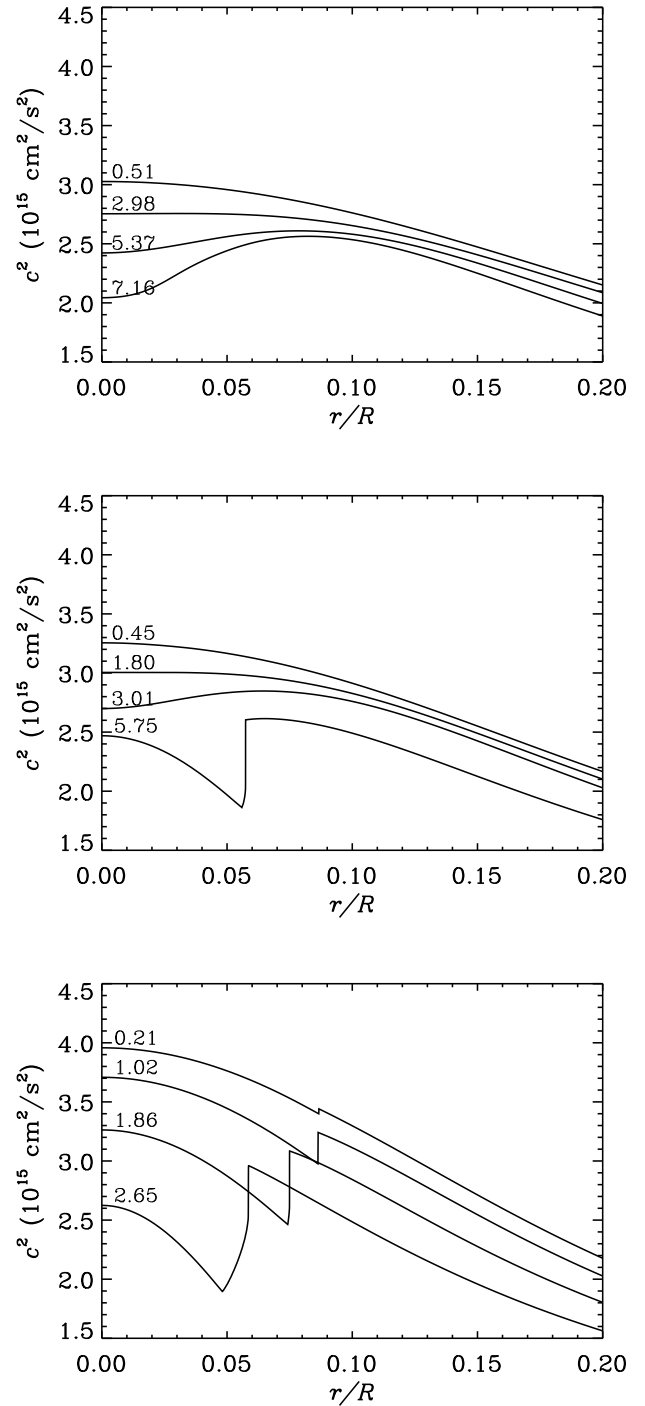


Figure 5. The sound-speed profile in the inner layers of a $M = 1.0 M_{\odot}$ (upper panel), $M = 1.1 M_{\odot}$ (middle panel) and $M = 1.4 M_{\odot}$ (lower panel) with different ages. The numbers at the beginning of the curves indicate the age of the models in Gyr. These models were computed with solar metallicity and assuming overshoot from the convective core of $\alpha_{OV} = 0.1$.

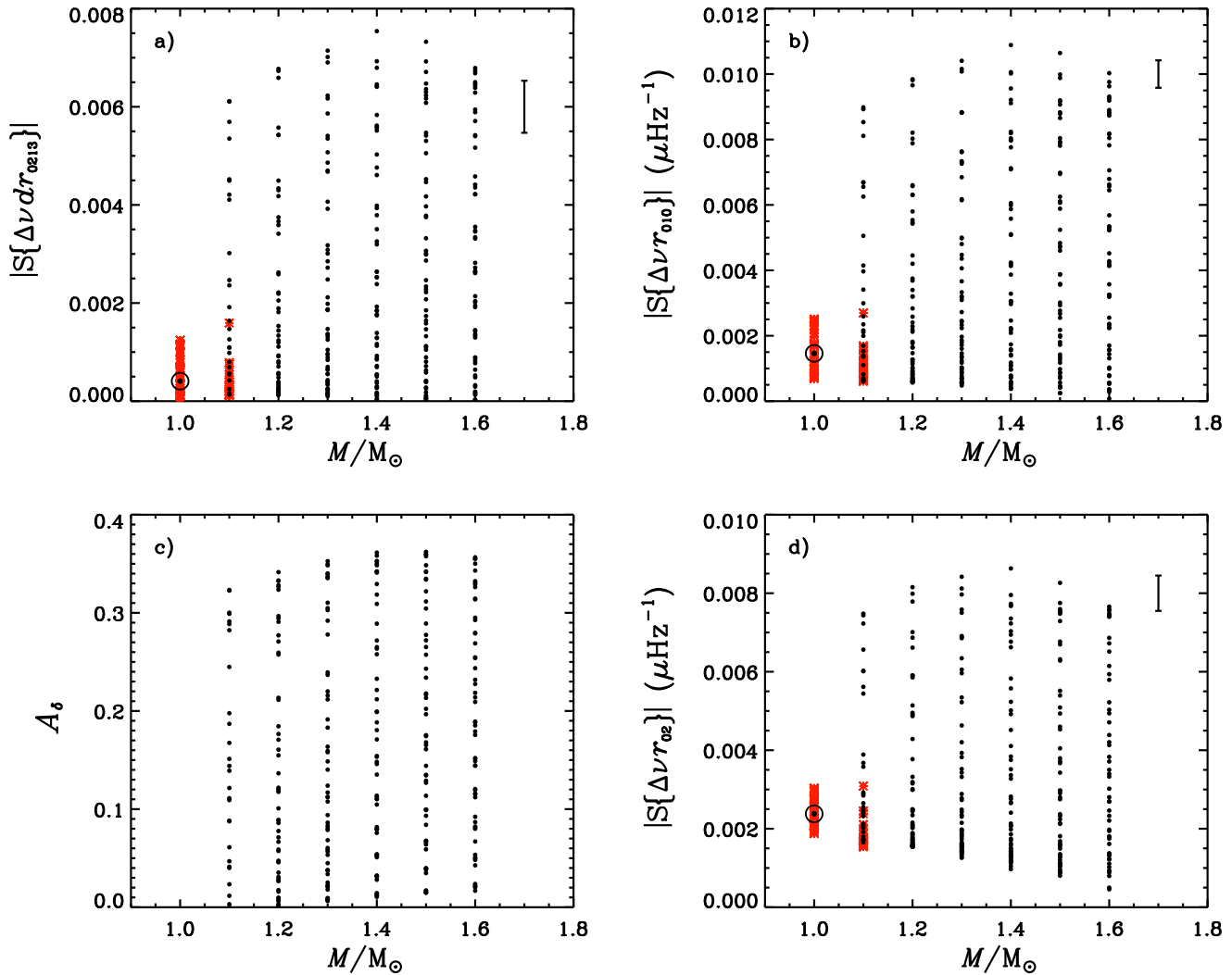


Figure 6. Panel (a): the symbols represent the absolute value of the slopes for the quantity $\Delta\nu dr_{0213}$, $|S\{\Delta\nu dr_{0213}\}|$, for all models considered as a function of the mass of the model. The red stars correspond to models with no convective core. The typical error bar for the slope of $\Delta\nu dr_{0213}$ is also shown in this plot. Panel (c) shows, for subset of models shown in panel (a) that have convective cores, the amplitude of the discontinuity as a function of the mass of the model. Panels (b) and (d) are similar to panel (a), but for the quantities $\Delta\nu r_{010}$ and $\Delta\nu r_{02}$, respectively. The symbol of the Sun shown at $M = 1.0 M_{\odot}$ represents the slopes of the diagnostic tools computed using the solar frequencies from Model S (Christensen-Dalsgaard et al. 1996).

4 RESULTS

4.1 Models with a convective core

Since our present study concerns only models with a convective core, we started by identifying which models in our grid are included in this category. We verified that no convective core exists in our $1.0 M_{\odot}$ sequences of main-sequence models. In Fig. 5, upper panel, we show an example of the sound-speed profile in the innermost regions of a sequence of $1.0 M_{\odot}$ models with solar metallicity. Clearly, these models do not show a sound-speed discontinuity, or even strong sound-speed gradients in the innermost layers, although an increase in the sound-speed gradient is seen as the model star evolves towards the terminal-age main sequence (TAMS). On the other hand, the presence or absence of a convective core in models with $1.1 M_{\odot}$ depends on the metallicity considered. There are no models with a convective core in our lowest metallicity sequences of $1.1 M_{\odot}$, namely with $Z/X = 0.0079$. The most evolved

models with $1.1 M_{\odot}$ and with solar $Z/X = 0.0245$ metallicity show a convective core (Fig. 5, middle panel) and the $1.1 M_{\odot}$ models with high metallicity, $Z/X = 0.0787$, all have a convective core. Models with $M \geq 1.2 M_{\odot}$ all have convective cores (Fig. 5, lower panel).

4.2 Slopes versus discontinuity in sound speed

According to Cunha & Brandão (2011), the quantity dr_{0213} is related to the frequency perturbation $\delta\nu^c$ induced by the discontinuity in sound speed at the edge of the convective core by

$$\delta\nu^c \sim \Delta\nu_{n-1,1} dr_{0213}. \quad (8)$$

Moreover, from the author's analysis it results that

$$\delta\nu^c \sim -F A_{\delta}, \quad (9)$$

where F is a function that depends on frequency, as well as on the shape of the sound speed around the discontinuity.

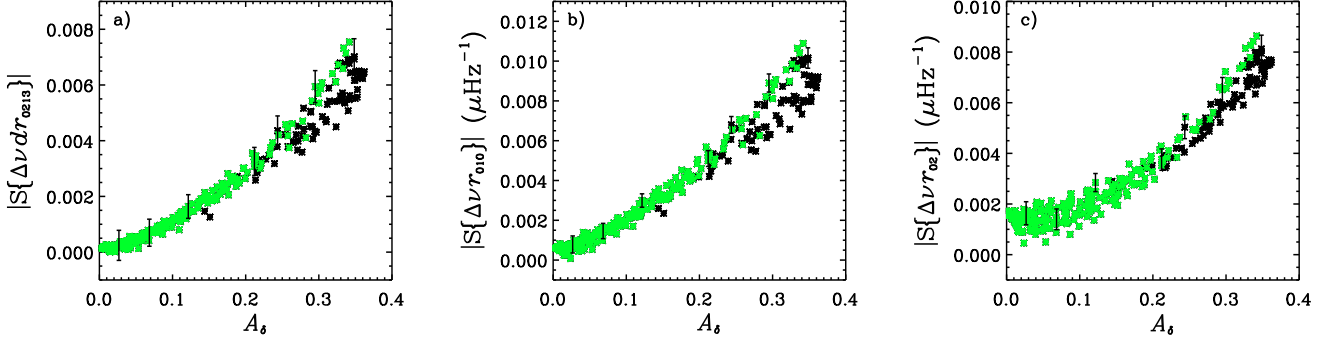


Figure 7. The absolute value of the slopes of the diagnostic tools $\Delta\nu dr_{0213}$ (panel a), $\Delta\nu r_{010}$ (panel b) and $\Delta\nu r_{02}$ (panel c) as a function of the relative amplitude A_δ of the squared sound speed. Each point represented by a star symbol, either black or green, corresponds to one model of our grids. Only models with a convective core are shown. These include models with masses between 1.1 and $1.6 M_\odot$ (see Section 4.1 for details). The green stars represent the subset of models for which the slope of the diagnostic tools was measured between ν_{\max} and ν_c (see Section 4.3 for details). The error bars shown were computed for some of the models of our grid.

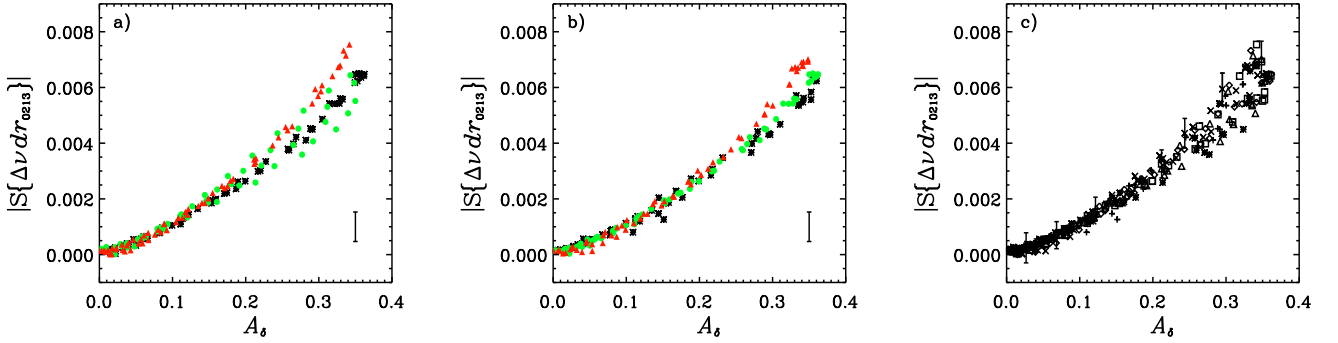


Figure 8. Panel (a): the absolute value of the slopes of the diagnostic tool $\Delta\nu dr_{0213}$ as a function of the relative amplitude A_δ of the discontinuity in the squared sound speed. The black stars represent models with solar metallicity, $Z/X = 0.0245$, the green filled circles represent models with $Z/X = 0.0079$, and the red triangles represent models with $Z/X = 0.0787$. The models have $\alpha_{\text{OV}} = 0.1$. The typical error bar for $|S\{\Delta\nu dr_{0213}\}|$, is shown in the lower right corner of the plot. Panel (b) shows the same quantities as in panel (a), but here the black stars represent models without overshoot, $\alpha_{\text{OV}} = 0.0$, the green filled circles represent models with $\alpha_{\text{OV}} = 0.1$ and the red triangles represent models with $\alpha_{\text{OV}} = 0.2$. The models have $Z/X = 0.0245$. Panel (c) also shows the same quantities as in panel (a) but here the different symbols correspond to different values of the mass, namely $M = 1.1 M_\odot$ are represented by crosses, $M = 1.2 M_\odot$ by stars, $M = 1.3 M_\odot$ by triangles, $M = 1.4 M_\odot$ by squares, $M = 1.5 M_\odot$ by diamonds and $M = 1.6 M_\odot$ by X. The error bars for $|S\{\Delta\nu dr_{0213}\}|$ in this case are shown for some models.

Let's now consider the quantity $S\{\Delta\nu dr_{0213}\}$ previously defined. Then, we have,

$$S\{\Delta\nu dr_{0213}\} \approx \left[\frac{d}{d\nu} (\Delta\nu dr_{0213}) \right]_{\nu_{\text{slope}}}, \quad (10)$$

where the derivative of the diagnostic tool $\Delta\nu dr_{0213}$ is to be taken at a place where F varies linearly with ν (which is approximately true at the frequency ν_{slope} where the slope is computed) and where $\Delta\nu$ is the average large separation for modes of degree $l = 1$ in the frequency range where the derivative is to be taken. From relations (8) and (9), one thus expects that $|S\{\Delta\nu dr_{0213}\}|$ provides a measure of the sound-speed discontinuity at the edge of any core.

In Fig. 6(a), we show $|S\{\Delta\nu dr_{0213}\}|$ computed for all models within our sequence of evolutionary tracks, as a function of the mass of the models. Models without a convective core are shown by the asterisk symbol in red. Fig. 6(c) shows the amplitude A_δ of the discontinuity in the squared sound speed as a function of the mass of the models. Note that no stars of $M = 1.0 M_\odot$ are shown

in this plot, because these stars do not have convective cores, and hence have no discontinuity in the sound speed. From panel (a) of this figure, we can see that for the physics considered in the models, $|S\{\Delta\nu dr_{0213}\}|$ is no higher than ~ 0.008 , independently of the mass of the models. This maximum value of ~ 0.008 is associated with a maximum value for A_δ of ~ 0.4 , which occurs when stars approach the TAMS and have a core essentially composed of helium. The existence of these maxima results from the fact that the variation of the mean molecular weight at the edge of the core is itself limited.

In Fig. 6(a), we can also see that models with $|S\{\Delta\nu dr_{0213}\}| \geq 0.002$ all have a convective core, while models with $|S\{\Delta\nu dr_{0213}\}| \leq 0.002$ may or may not have a convective core, depending on the mass. Therefore, for a given observation of a star, if we find that $|S\{\Delta\nu dr_{0213}\}| \geq 0.002$, we can say with confidence that the star has a convective core.

If the $l = 3$ modes are not observed, the two diagnostic tools d_{010} and d_{02} , or their respective ratios, which consider modes of degree only up to 2 should be preferred. Note, however, that these

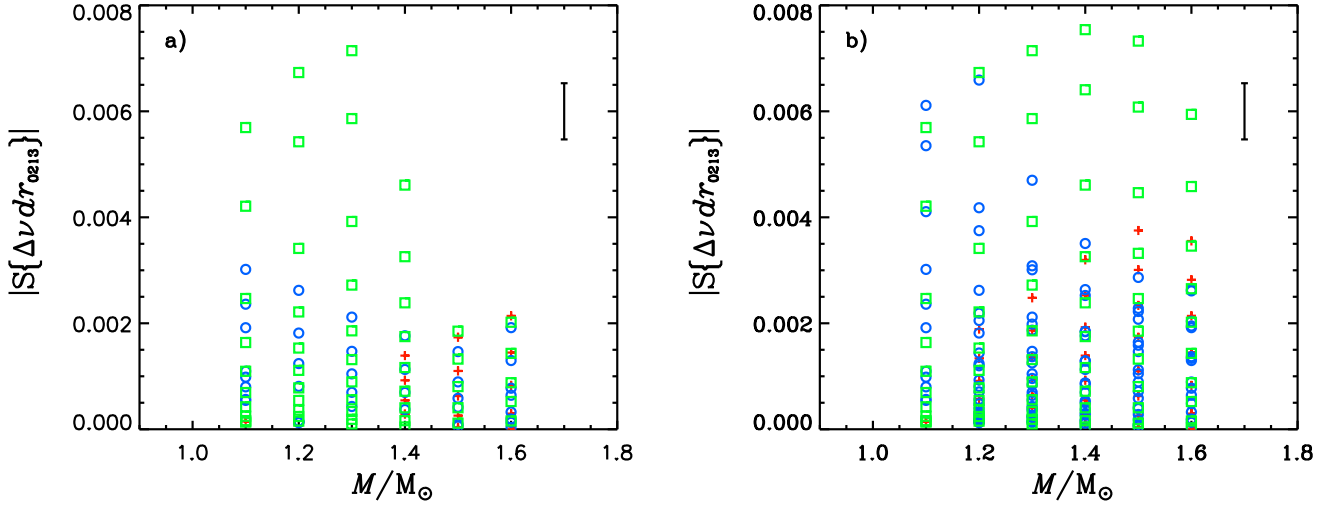


Figure 9. The same as in Fig. 6(a) but considering only models for which the frequency region where the slopes are computed is between $\nu_{\max} - 8\Delta\nu$ and $\nu_{\max} + 8\Delta\nu$ (panel a) or between ν_{\max} and ν_c (panel b). The different symbols represent different metallicities, namely red crosses represent $Z/X = 0.0079$, blue circles represent $Z/X = 0.0245$ and green squares represent $Z/X = 0.0787$.

two quantities measure differently the structure of the core; hence, unlike dr_{0213} , they do not isolate the signature of the sharp structural variation in the sound speed. As a consequence, when using these two diagnostic tools one should have in mind that the effect of a much wider region of the star, and not only the discontinuity, is present. Nevertheless, it is interesting to see that when analysing the slopes of $\Delta\nu r_{02}$ and $\Delta\nu r_{010}$ we obtain results that are analogous to the ones previously mentioned for the diagnostic tool $\Delta\nu dr_{0213}$. We verified that $|S\{\Delta\nu r_{010}\}|$ and $|S\{\Delta\nu r_{02}\}|$ are also bounded, in this case by maximum values of 0.011 and $0.009 \mu\text{Hz}^{-1}$, respectively (cf. Fig. 6 panels b and d). Moreover, models with $|S\{\Delta\nu r_{010}\}| \geq 0.003 \mu\text{Hz}^{-1}$ or $|S\{\Delta\nu r_{02}\}| \geq 0.0035 \mu\text{Hz}^{-1}$ all have convective cores. So, as before, for these two quantities, we are confident that a detection of a slope with absolute value larger than $\sim 0.0035 \mu\text{Hz}^{-1}$ is a strong indication of the presence of a convective core.

Next, we investigate in more detail the relation between the slopes and the amplitude of the discontinuity. If the function F were model independent, then one would expect $|S\{\Delta\nu dr_{0213}\}| \propto A_\delta$, i.e., one would expect a linear relation between $|S\{\Delta\nu dr_{0213}\}|$ and A_δ . However, the fact that F is model-dependent means that deviations from a simple linear relation, as well as significant dispersion, may exist in the relation between these two quantities.

In Fig. 7(a), we show the relation between the absolute value of the slopes computed for the diagnostic tool $\Delta\nu dr_{0213}$, $|S\{\Delta\nu dr_{0213}\}|$, and the relative amplitude A_δ of the discontinuity in the squared sound speed. As anticipated from the work of Cunha & Brandão (2011), there is a strong dependence of the slopes on the amplitude of the discontinuity. Nevertheless, that relation deviates from linear and shows significant dispersion, particularly for larger values of A_δ . This may be explained by the fact that as the star approaches the TAMS, the sound-speed perturbation becomes wider (cf. Fig. 5, bottom panel) and the model dependence of the function F becomes more evident.

In fact, for the younger stars with $A_\delta \leq 0.2$, the relation shown in panel a) of Fig. 7 was found not to depend significantly on the mass, core overshoot or metallicity, at least for the physics that we considered in our set of models. However, at latter stages, that is no longer the case. To illustrate this, we show, in Fig. 8(a), the depen-

dence of the relation between $|S\{\Delta\nu dr_{0213}\}|$ and A_δ on the metallicity. In Fig. 8(b) we show the dependence of the same relation on the overshoot and, finally, in Fig. 8(c) we show the dependence on the mass. A dependence of the relation on metallicity and overshoot clearly emerges as the stars approach the TAMS. On the other hand, no clear dependence on stellar mass is seen even at the latest evolution stages.

In Figs. 7(b) and (c), we show the same relation as before, but for the quantities $\Delta\nu r_{010}$ and $\Delta\nu r_{02}$, respectively. Although the two latter diagnostic tools do not isolate the effect of the discontinuity in the sound speed, the similarity with the plot for the first diagnostic tool, particularly for the case of $\Delta\nu r_{010}$, indicates that their slopes are strongly affected by this discontinuity.

4.3 Diagnostic potential

To establish the relations discussed in Section 4.2, between the absolute value of the slopes of the diagnostic tools and the amplitude of the discontinuity in the squared sound speed, we have considered all models in our grid. However, as mentioned earlier, for a number of models, the frequency at which the slope is computed is not in the range of observed frequencies. For instance, for a typical main-sequence solar-like pulsator observed by the *Kepler* satellite, only about a dozen of radial orders, centred on ν_{\max} , are observed.

To illustrate the impact of these observational limitations, we have considered two subset of models, namely (1) a subset composed of models for which the frequency region where the slopes are computed is between $\nu_{\max} - 8\Delta\nu$ and $\nu_{\max} + 8\Delta\nu$ and (2) a subset composed of models for which the frequency region where the slopes are computed is between ν_{\max} and ν_c . They contain, respectively, 35 and 74 per cent of the total number of stars with a convective core in our sample. These percentages increase to 49 and 98 per cent of the models in our sample, respectively, when we consider only models with a convective core and $A_\delta \leq 0.2$.

We show in Fig. 9 again the plot present in Fig. 6(a) but considering only models for which the frequency region where the slopes are computed is between $\nu_{\max} - 8\Delta\nu$ and $\nu_{\max} + 8\Delta\nu$ (panel a) or between ν_{\max} and ν_c (panel b). The different metallicities consid-

ered in the models are shown with different symbols. Models with $|S\{\Delta v dr_{0213}\}| \gtrsim 0.003$ and for which the frequency region where the slopes are computed is between $\nu_{\max} - 8\Delta\nu$ and $\nu_{\max} + 8\Delta\nu$ all have the highest metallicity, namely $Z/X = 0.0787$.

In Fig. 7, the green symbols represent the models for which the slope of the diagnostic tools was measured between ν_{\max} and ν_c . Clearly, when considering only the subset of models for which the frequency region where the slopes are computed may be observed, the dispersion in the relation between the slopes of the diagnostic tools and the amplitude of the discontinuity in the sound speed squared seen earlier for the more evolved models is significantly reduced. Thus, from our results we may conclude that it is possible, for a significant subset of stars, to get a measure of the amplitude of the discontinuity in the sound speed from the analysis of the observed oscillation frequencies. Nevertheless, we note that this subset is either strongly biased towards stars in first half of their main-sequence lifetime or towards stars with large metallicity.

One would hope that the measurement of the discontinuity in the sound speed could be related to the evolutionary state of the star. To test this possibility, we inspected directly the relation between the slopes of the different diagnostic tools and the star's fraction of evolution (t/t_{TAMS}) along the main sequence, where t is the age of the star at a given evolutionary stage in the main sequence and t_{TAMS} is the age of the star within the same evolutionary track but at the TAMS. We considered the stellar fraction of evolution and not the stellar age alone since the latter is strongly dependent on the stellar mass. Fig. 10 shows, for all models with a convective core and for which the frequency region where the slope is computed is between ν_{\max} and ν_c , the absolute value of the slopes of $\Delta v dr_{0213}$, $|S\{\Delta v dr_{0213}\}|$, as a function of the fraction of main-sequence stellar evolution, t/t_{TAMS} . By inspecting this figure, we see a large spread in the slopes at the higher evolution fractions, namely at $t/t_{\text{TAMS}} \gtrsim 0.6$. This is due to the fact that models with $M = 1.1 M_{\odot}$, solar metallicity and $\alpha_{\text{OV}} = 0.0$ have a very small central convective region. As a result, substantial conversion of hydrogen into helium takes place outside the inner convective region and, in turn, the discontinuity in the chemical composition at the edge of that convective region is significantly smaller than in otherwise similar models with overshoot, at the latest stages of evolution. This is illustrated in Fig. 11 where we compare the cases of models with $M = 1.1 M_{\odot}$ and solar metallicity and different values for the overshoot parameter. Moreover, we find that, for a similar reason, models with $M = 1.2 M_{\odot}$ and no overshoot still have a relatively small convective core, hence a slope still smaller than that of similar mass models with overshoot or models of higher mass at the later stages of their evolution.

One interesting consequence of this overshoot-dependent slope dispersion seen in the lower mass models of our grid is that it opens the perspective of constraining the extent of overshoot present at the border of convective regions in stars based on the analysis of the slopes, if the stellar mass can be accurately estimated.

In fact, for relatively evolved $M = 1.1 M_{\odot}$ models with solar metallicity, the slopes depend strongly on overshoot and a measurement of a relatively large absolute value for the slope in a star at such mass would imply the presence of significant overshoot.

Fig. 12, upper panel, shows the same plot as in Fig. 10 but for models with $M \gtrsim 1.3 M_{\odot}$ only. The dispersion seen in this case is significantly smaller than in Fig. 10 because these higher mass models have a relatively large convective-core region and, thus, show the expected age- A_s relation, even when $\alpha_{\text{OV}} = 0$. Fig. 12, middle and lower panels show, respectively, the absolute value

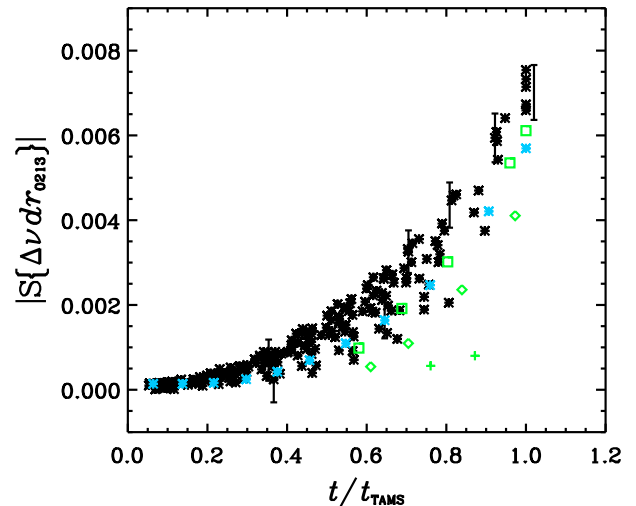


Figure 10. The absolute value of the slopes of the diagnostic tool $\Delta v dr_{0213}$, $|S\{\Delta v dr_{0213}\}|$, as a function of the fraction of stellar evolution, t/t_{TAMS} , for the models of our grid that have a convective core and for which the frequency region where the slopes are computed is between ν_{\max} and ν_c . These are all models with $1.2 \leq M \leq 1.6 M_{\odot}$ and models with $M = 1.1 M_{\odot}$ with metallicities $Z/X = 0.0245$ (green symbols) and $Z/X = 0.0787$ (light blue stars). The different symbols in green represent different values for the overshoot parameter, namely $\alpha_{\text{OV}} = 0.0$ (crosses), $\alpha_{\text{OV}} = 0.1$ (diamonds) and $\alpha_{\text{OV}} = 0.2$ (squares).

of the slopes of the diagnostic tools $\Delta v r_{010}$ and $\Delta v r_{02}$, as a function of the fraction of evolution, for the models with $M \gtrsim 1.3 M_{\odot}$. From these, we may conclude that for relatively massive solar-like pulsators ($M \gtrsim 1.3 M_{\odot}$), some direct constraints to the fraction of evolution along the main-sequence can be derived by inspecting the slopes of the diagnostic tools considered here, in particular the $\Delta v dr_{0213}$ and the $\Delta v r_{010}$.

Such constraints are stronger for relatively evolved stars, when the age dependence of the slopes is more accentuated. However, in this case they are limited to metallic stars, since only for those one may observe the frequency region where the slope is computed.

5 CONCLUSIONS

We performed a systematic study of the slopes of the diagnostic tools dr_{0213} , r_{010} and r_{02} , where the slopes are defined as the frequency derivatives of these quantities taken at their maximum absolute value. For this study, we considered stellar models of different masses, metallicities and convective-core overshoots and at different evolutionary states in the main sequence.

We verified that for each evolutionary sequence, the absolute value of the slopes increases as the star evolves on the main sequence. This increase is associated with the increase in the sound-speed discontinuity at the edge of the core. We determined, for each diagnostic tool, the maximum absolute value that the slope may take and provided evidence that these maxima result from the existence of a maximum discontinuity in the mean molecular weight. The maximum absolute values that we found for the slopes of $\Delta v dr_{0213}$, $\Delta v r_{010}$ and $\Delta v r_{02}$ were, respectively, ~ 0.008 , ~ 0.011 and $\sim 0.009 \mu\text{Hz}^{-1}$. Thus, if one such slope is found in a star, one can confidently assume that the star is very close to the TAMS.

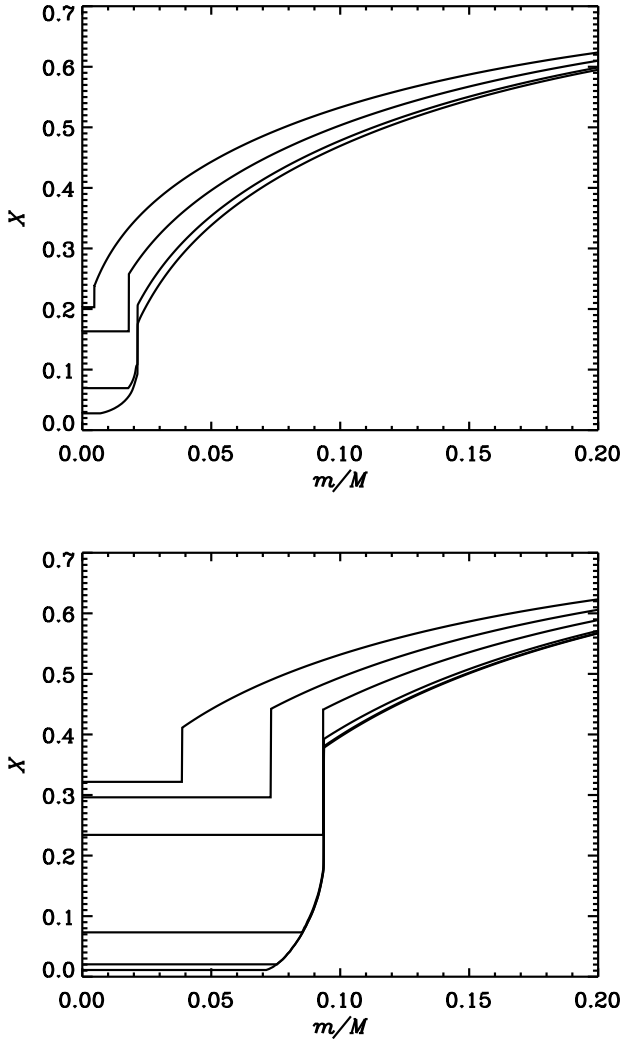


Figure 11. The hydrogen profile of a $M = 1.1 M_{\odot}$ model with $Z/X = 0.0245$ and with $\alpha_{OV} = 0.0$ (upper panel) and a $M = 1.1 M_{\odot}$ model with $Z/X = 0.0245$ and with $\alpha_{OV} = 0.2$ (lower panel). The different curves correspond to different stages of evolution. Only models with a convective core are shown.

In addition, we found that models with $|S\{\Delta\nu dr_{0213}\}| \geq 0.002$, $|S\{\Delta\nu r_{010}\}| \geq 0.003 \mu\text{Hz}^{-1}$ and $|S\{\Delta\nu r_{02}\}| \geq 0.0035 \mu\text{Hz}^{-1}$ all have convective cores. Within these models, those for which the measured slope is in the expected observed frequency range, namely between $\nu_{\max} - 8\Delta\nu$ and $\nu_{\max} + 8\Delta\nu$, are the most metallic ones, with $Z/X = 0.0787$. Models with $|S\{\Delta\nu dr_{0213}\}| \lesssim 0.002$, $|S\{\Delta\nu r_{010}\}| \lesssim 0.003 \mu\text{Hz}^{-1}$ and $|S\{\Delta\nu r_{02}\}| \lesssim 0.003 \mu\text{Hz}^{-1}$ may or may not have a convective core, depending on the mass.

For all diagnostic tools, we found a strong correlation between the slopes and the relative amplitude A_{δ} of the discontinuity in the squared sound speed. We thus conclude that when the slopes of the diagnostic tools can be computed from the observations, they provide a direct measurement of the relative amplitude of the sound-speed discontinuity at the edge of the core. We note, however, that the slopes, as defined in this work, can only be computed in practice for stars in which the range of observed frequencies contains the frequency where the derivative of the diagnostic tools reach their

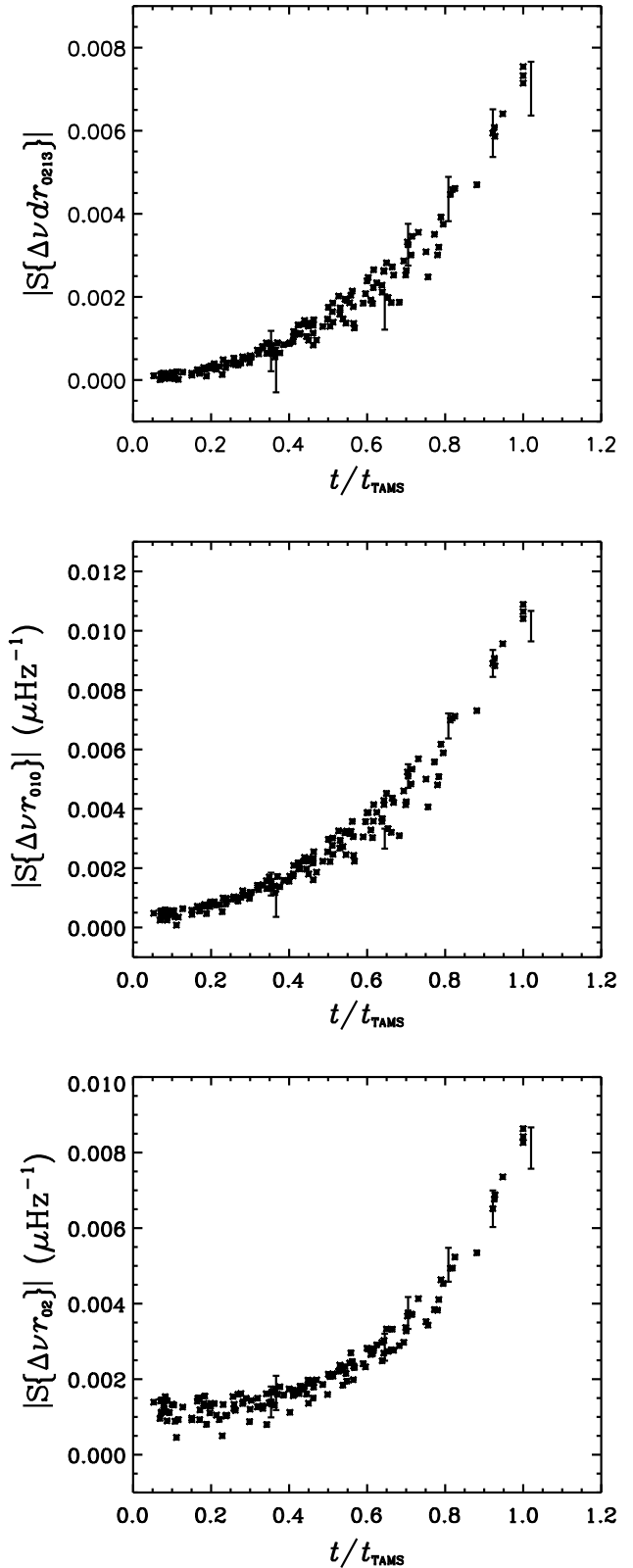


Figure 12. Upper panel: the same as in Fig. 10 but here only considering models with $M \geq 1.3 M_{\odot}$. The same models are shown in the middle and lower panels for the slopes of the diagnostic tools $\Delta\nu r_{010}$ and $\Delta\nu r_{02}$, respectively.

maximum absolute value. We have shown that at least 35 per cent of stars in our sample are expected to satisfy this condition.

Finally, we considered in more detail the relation between the slopes of the diagnostic tools and the fraction of stellar main-sequence evolution, t/t_{TAMS} . This relation is stronger for the diagnostic tools dr_{0213} and r_{010} than for r_{02} . Also, the dispersion seen in these relations is significantly reduced when only models with masses $M \geq 1.3 M_{\odot}$ are considered. For these masses, one may thus be able to use the slopes of dr_{0213} or r_{010} to infer about t/t_{TAMS} , at least for stars in which the slope can be computed from the observations. On the other hand, for stars with masses $M \leq 1.2 M_{\odot}$, the dispersion seen in the slope versus t/t_{TAMS} relation was found to be directly related to the amount of core overshoot, which in these lower mass stars, with very small convective cores, influences the amplitude of the discontinuity in the mean molecular weight at fixed evolutionary stage. As a consequence, for these lower mass stars, it may be possible to use the slopes to discriminate against models with small amounts of core overshoot.

ACKNOWLEDGMENTS

IMB acknowledges the support from the Fundação para a Ciência e Tecnologia (Portugal) through the grant SFRH/BPD/87857/2012. MSC is supported by an Investigador FCT contract funded by FCT/MCTES (Portugal) and POPH/FSE (EC). IMB and MSC acknowledge the support from ERC, under FP7/EC, through the project FP7-SPACE-2012-312844. Funding for the Stellar Astrophysics Centre is provided by The Danish National Research Foundation (Grant DNR106). The research is supported by the ASTERISK project (ASTERoseismic Investigations with SONG and Kepler) funded by the European Research Council (grant agreement no.: 267864).

REFERENCES

- Angulo C. et al., 1999, Nucl. Phys. A, 656, 3
 Böhm-Vitense E., 1958, Z. Astrophys., 46, 108
 Borucki W. J. et al., 2010, Science, 327, 977
 Casagrande L., 2007, in Vallenari A., Tantaló R., Portinari L., Moretti A., eds, ASP Conf. Ser., Vol. 374, From Stars to Galaxies: Building the Pieces to Build Up the Universe. Astron. Soc. Pac., San Francisco, p. 71
 Christensen-Dalsgaard J., 1984, in Mangeney A., Praderie F., eds, Space Research in Stellar Activity and Variability. Observatoire de Paris-Meudon, Paris, p. 11
 Christensen-Dalsgaard J., 2008a, Ap&SS, 316, 13
 Christensen-Dalsgaard J., 2008b, Ap&SS, 316, 113
 Christensen-Dalsgaard J. et al., 1996, Science, 272, 1286
 Christensen-Dalsgaard J., Gough D. O., Morgan J. G., 1979a, A&A, 73, 121
 Christensen-Dalsgaard J., Gough D. O., Morgan J. G., 1979b, A&A, 79, 260
 Cunha M. S., Brandão I. M., 2011, A&A, 529, A10
 Cunha M. S., Metcalfe T. S., 2007, ApJ, 666, 413
 Faulkner D. J., Cannon R. D., 1973, ApJ, 180, 435
 Ferguson J. W., Alexander D. R., Allard F., Barman T., Bodnarik J. G., Hauschildt P. H., Heffner-Wong A., Tamanai A., 2005, ApJ, 623, 585
 Gough D. O., 1983, in Shaver, P. A. and Kunth, D. and Kjar, K., eds, Primordial Helium. ESO, Garching, p. 117
 Grevesse N., Noels A., 1993, in Kubono S., Kajino T., Origin and Evolution of the Elements. Cambridge Univ. Press, Cambridge, p. 14
 Iglesias C. A., Rogers F. J., 1996, ApJ, 464, 943
 Mitalas R., 1972, ApJ, 177, 693
 Oti Floranes H., Christensen-Dalsgaard J., Thompson M. J., 2005, MNRAS, 356, 671
 Ribas I., Jordi C., Giménez Á., 2000, MNRAS, 318, L55
 Rogers F. J., Nayfonov A., 2002, ApJ, 576, 1064
 Roxburgh I. W., 2005, A&A, 434, 665
 Roxburgh I. W., Vorontsov S. V., 2003, A&A, 411, 215
 Roxburgh I. W., Vorontsov S. V., 2004, in Favata F., Aigrain S., Wilson A., eds, ESA SP-538: Stellar Structure and Habitable Planet Finding. ESA, Noordwijk, Vol. 538, p. 403
 Saio H., 1975, Sci. Rep. Tokohu Univ. Eighth Ser., 58, 9
 Serenelli A. M., Basu S., 2010, ApJ, 719, 865
 Silva Aguirre V. et al., 2013, ApJ, 769, 141
 Vernazza J. E., Avrett E. H., Loeser R., 1976, ApJS, 30, 1